# Experimental Investigation of Flow Characteristics of a Magnetohydrodynamic (MHD) Duct of Fan-Shaped Cross Section

**Seong Jae Kim*, Choung Mook Lee** and Sang Joon Lee*****

(*Received March 28, 1996*)

Experiments along with numerical calculations are carried out to investigate the effect of the geometry of the cross section on flow characteristics of a MHD propulsion duct. A fan-shaped cross-section MHD thruster duct is chosen for comparison with a previously investigated rectangular cross section. Measurement of the velocity field is made using LDV (Laser Doppler Velocimetry) system with a fiber-optic cable and pressure distribution is measured with static pressure holes at the bottom surface. Comparison with rectangular cross section shows that the velocity profile is significantly influenced by the geometry of cross section while the axial pressure distribution is not so affected.

**Key Words:** MHD Flows, MHD Ship Propulsion

## 1. Introduction

Currently used marine propellers can induce vibration, noise and cavitations, which are undesirable features associated with marine propellers. The propeller system requires some heavy mechanical devices such as shaft, bearings, and supporting stands which consume a significant amount of energy.

Above shortcomings of propeller have made many researchers to search for alternative marine propulsion systems. One of such propulsions is the MHD (Magnetohydrodynamic) propulsion for ships of high speed and quietness. The concept of the MHD propulsion was pursued by the investigations in the United States in 1960's (Rice, 1961; Friauf, 1961; Phillips, 1962; Doragh, 1963; Way, 1968) followed by the people in Japan since late 1970's (Iwata et al., 1978).

The first real sea trial was made with YAMATO-1 in 1992 by Japan Ship & Ocean Foundation. It had the total displacement of 180tons, 30 m in length, 7.8kN of thrust force and maximum speed of 4 m/s. The maximum magnetic field strength was 4T. The ship had twin internal DC type thrusters. Its thrust efficiency was 1.7% which is way too low to compete with the conventional propulsion systems; however, it was an important progress in MHD propulsion.

As discussed by the previous investigators, a superconducting magnet which can generate high magnetic flux density is indispensable for the development of MHD propulsion ship of high efficiency. If a superconducting magnet which can function in liquid nitrogen, which may be realized within a decade or two, can be available in the future, the development in MHD propulsion will be considerably accelerated.

## 2. Objective and Approach

In application of MHD to marine propulsion, investigations of a variety of physical phenomena should be carried out including the flow characteristics in a MHD duct, thrust efficiency, optimum shape of the duct, and problems including electrolysis along with non-corrosion electrodes, and, most of all, superconducting magnet.

In the present work, the investigation is limited

* Graduate Student, Department of Mechanical Engineering, Postech
** Professor, Department of Mechanical Engineering, Postech
*** Associate Professor, Department of Mechanical Engineering, Postech

to the flow characteristics in a MHD duct of a fan-shaped cross section. The flow characteristics is investigated through experiments and computations. The present investigation is to determine the effect of the cross-sectional geometry, different from the previously investigated rectangular cross section, on the MHD thrust duct flow. The pressure and velocity distribution characteristics of the duct are investigated and compared with the previous results of a rectangular cross-section duct (Kim, 1995).

## 3. Principles of MHD Propulsion

When intersecting electric and magnetic fluxes are applied to a conducting fluid, the fluid is forced to the direction perpendicular to the plane where magnetic and electric fluxes are intersecting. The thrust force is called the Lorentz force. The Lorentz force $f_L$ acts as a body force in the momentum equation for an incompressible fluid as follows:

$$\frac{\partial \boldsymbol{u}}{\partial t}+\boldsymbol{u}\cdot\nabla\boldsymbol{u}=-\frac{1}{\rho}\nabla p+\nu\nabla^2\boldsymbol{u}+\boldsymbol{f}_L \qquad (1)$$

where $\boldsymbol{f}_L=\frac{1}{\rho}\boldsymbol{J}\times\boldsymbol{B}$ and $\boldsymbol{u}$ is the velocity vector, $p$ the pressure, $\nu$ the kinematic viscosity, $\rho$ the density of sea water, $\boldsymbol{J}$ the electric-flux density vector and $\boldsymbol{B}$ the magnetic-flux density vector.

The coordinate system to be employed in the present analysis is a right-handed Cartesian coordinate system which is shown in Fig. 1.

In steady state, with z-directional electric field and y-directional magnetic field, the x-component of Eq. (1) is

$$u\frac{\partial u}{\partial x}+v\frac{\partial u}{\partial y}+w\frac{\partial u}{\partial z}=-\frac{1}{\rho}\frac{\partial p}{\partial x}+\nu\left(\frac{\partial^2 u}{\partial x^2}+\frac{\partial^2 u}{\partial y^2}+\frac{\partial^2 u}{\partial z^2}\right)+\frac{1}{\rho}J_zB_y \qquad (2)$$

where

$$J_z=\sigma(E_z-uB_y) \qquad (3)$$

and $\sigma$ is the electric conductivity of sea water, $E_z$ the electric field intensity, and the subscripts y and z indicate the respective vector components.

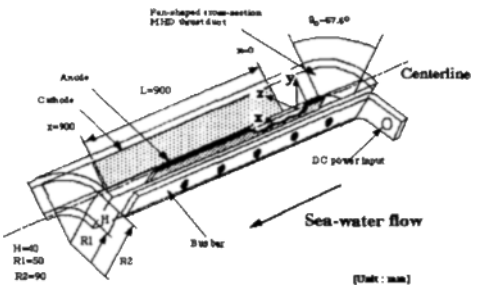


**Fig. 1** Fan-shaped cross-section MHD thrust duct

In Eqs. (2) and (3), $E_z$ and $B_y$ are the absolute values of each component.

In a practical application, it is found that $E_z \gg uB_y$ and, in the present invesitgation, the characteristic electric field intensity $E_z$ and the product of the characteristic velocity and magnetic flux density $uB_y$ are as follows:

$$E_z=731(V/m),\quad uB_y=0.3(V/m)$$

If we set the orders of magnitude of $E_z$ and $B_y$ as $O(1)$, with the condition of $E_z \gg uB_y$, the order of magnitude of $u$ is $O(\varepsilon)$ $\varepsilon \ll 1$. Therefore, the convection term and diffusion term of Eq. (2) are sufficiently small in magnitude compared to the rest of the terms and can be neglected. Then, the relation of the pressure gradient in longitudinal direction and the applied electromagnetic force is simplified as

$$\frac{\partial p}{\partial x}=J_zB_y=\sigma E_zB_y \qquad (4)$$

From Eq. (4), it can be seen that the Lorentz force applied to a conducting fluid increases the pressure of the flow field linearly along the direction of the flow movement. Integration over the length of the region under the Lorentz force becomes

$$\Delta p=J_zB_yL_x \qquad (5)$$

where $L_x$ represents the length along the direction of the flow movement under the influence of Lorentz force.

Non-dimensional MHD flow parameters in the present investigation are

Interaction parameter:

$$N=\frac{\sigma B_o^2 L}{\rho U}=\frac{(4)\,(0.5)^2(0.051)}{(1025)\,(0.6)}$$
$$=8.27\times10^{-5} \quad (6)$$

Hartmann number:

$$Ha=\sqrt{N\cdot Re}=\sqrt{(8.27\times10^{-5})\,(29400)}$$
$$=1.56 \quad (7)$$

Magnetic Reynolds number:

$$Re_m=\mu\sigma UL$$
$$=(4\pi\times10^{-7})\,(4)\,(0.6)\,(0.051)$$
$$=1.54\times10^{-7} \quad (8)$$

where $B_o$ is the characteristic magnetic flux density, $L$ the characteristic length, $\mu$ the magnetic permeability of sea water.

## 4. Numerical Calculation

In the present investigation, numerical calculation for the fan-shaped MHD duct flow is carried out. The computer code used in the present calculation was developed for solving MHD flow by Kim (1995) based on the CNS-3D (Chen, 1986) code which can solve the curvilinear Navier-Stokes equations in three-dimensional space. A body fitted coordinate (BFC) system is adopted and arbitrary geometries can be numerically processed by the code. Standard $k-\varepsilon$ model (Launder and Spalding, 1972) for the Reynolds stresses in MHD flow is used to calculate turbulent flows. Magnetic field fluctuation is not considered in the present analysis because, as shown in Eq. (8), Magnetic Reynolds number is sufficiently small and this means the fluctuation of the flow field does not affect the magnetic field.

Solution procedure for the discretized equations is based on the velocity-pressure correction algorithm, SIMPLE-C. Staggered grid systems are used to prevent the difficulties in solving the wavy pressure or velocity field.

In the calculation, the assumption of steady flow and incompressible fluid is made. Dimensions of the solution domain are the same with the experimental fan-shaped, cross-section duct. In solving the flow field, uniform inlet condition and fully developed outlet condition are used. No-slip condition is imposed on the walls of the duct.

In the case of the electric potential function, the Dirichlet boundary condition, $\phi=\phi_o$, is imposed on the electrode walls and the Neumann boundary condition, $\partial\phi/\partial n=0$, is imposed on the non-conducting duct walls.

## 5. Experimental Apparatus and Method

Figure 1 shows a schematic view of the fan-shaped, cross-section duct and Fig. 2 shows the cross section of the duct. The length, width at the mid-depth, and the depth of the duct will be denoted by $L$, $W$, and $H$, respectively.

As shown in Figs. 1 and 2, the origin of the coordinate is located at the start of the electrode and at the centerline of the bottom surface of the duct. The fluid flows in the positive $x$-direction and the electric and magnetic fields are generated, respectively, in the positive $z$-direction (circumferential) and in the negative $y$-direction. The Lorentz force is controlled by changing the

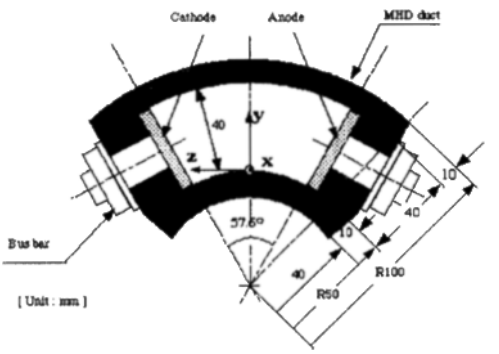


**Fig. 2** Cross section of the fan-shaped MHD propulsion duct

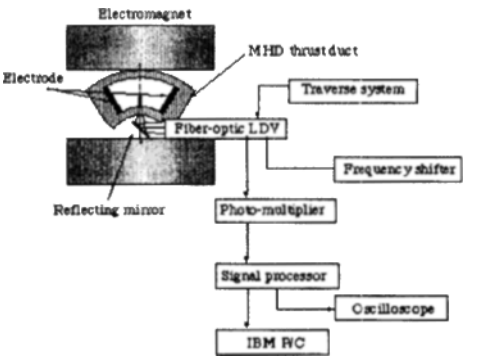


**Fig. 3** Schematic of the fiber-optic LDV measurement system

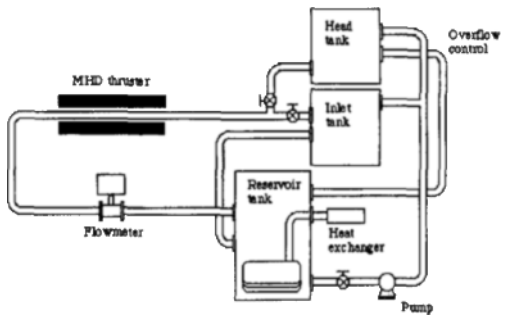


**Fig. 4** Schematic diagram of MHD thruster experimental flow loop

strengths of the electric and the magnetic fields.

Pressure distributions in the flow direction at the bottom surface of the thruster duct are measured with 14 pressure holes at intervals of 100 mm. Velocity profiles in the vertical direction are measured using the laser doppler velocimetry (LDV) system. Figure 3 shows the schematic of the present LDV velocity measurement system.

A dipole magnet was fabricated by winding a copper wire around a 0.25 % silicon containing lamination steel. The magnetic field power supply system can generate the magnetic flux density up to 1.1 $T$. Magnetic field was found uniform throughout the test section.

A pair of parallel electrodes was used in the experiment. The maximum electric field is 1096 V/m. The electric field in the longitudinal direction is uniform between two electrodes except at the ends of the electrodes. For the present electrodes, Iridium oxide of 5 mm thickness is coated for the anode on the titanium base to prevent the corrosion by sodium hypochloride. Platinum of 5 $\mu$m thickness is coated on the cathode.

The sea-water temperature in the MHD flow loop is increased by Joule heating between the two electrodes. The temperature increase of sea water is suppressed by using a 18 kW-capacity heat exchanger. The temperature change during the experiment was controlled within $\pm 1$ ℃. Figure 4 shows the present experimental MHD flow loop.

In the experiment, 4 W Argon laser was used and velocity measuring volume was formed by a fiber-optic LDV probe. Aluminum powder was used as the seeding particle, which yielded a sufficient signal to noise ratio. Aluminum has relative magnetic permeability of 1 H/m, so that the effect of the aluminum powder on the magnetic field can be neglected.

The laser source generates beams of three wave lengths of violet, blue and green. Among them, the green beam of $\lambda=514.5$ nm was used in the experiment.

The curved bottom surface through which the laser beam is passed for the velocity measurement was replaced with a window of a transparent narrow flat plate because the curvature of the wall impairs the velocity measurement. Three velocity measuring windows were installed at $x/L=0$, 0.6 and 1.0 along the longitudinal direction of the duct. Here $L$ means the electrode length.

## 6. Results and Discussion

### 6.1 Pressure distribution

Measurements were made in both cases of the zero initial velocity of seawater and of the initially onset flow using a head tank.

Figure 5(a) and (b) show the pressure distributions due to the Lorentz force in the case of zero initial velocity for the fan-shaped, cross-section duct where $I$ represents the electric current. The points where the static pressure kinks occur a little distance after the beginning of the electrode ($x/L=0$) for the case of $B=0.5T$ are due to the bubble layers which float over those pressure measuring points. Figure 5(a) and (b) show that the pressure increases linearly along the flow direction due to the Lorentz force as indicated by Eq. (6). The trend is more obvious as the strength of the Lorentz force is increased.

Figure 6(a) and (b) show the results of the pressure measurements in the case of initially onset flow. The onset flow was generated by the head tank using a flow-rate-control valve. In the initially onset flow case, it was observed that the flow-rate increase due to the Lorentz force was negligible. The pressure increase is clearly proportional to the applied Lorentz force. From the results shown in Figs. 5 and 6, it can be found that the pressure gradients are identical whether

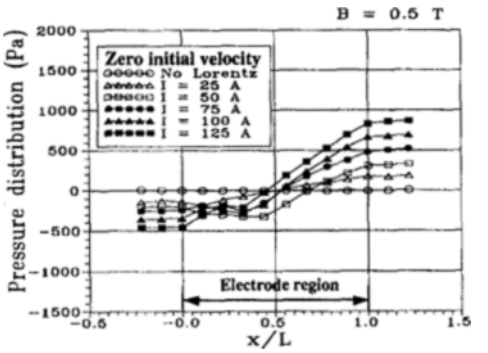


(a) B=0.5T

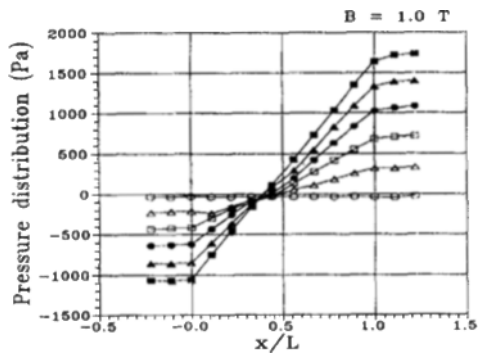


(b) B=1.0T

**Fig. 5** Pressure distribution in case of zero initial velocity of the fan-shaped MHD thrust duct

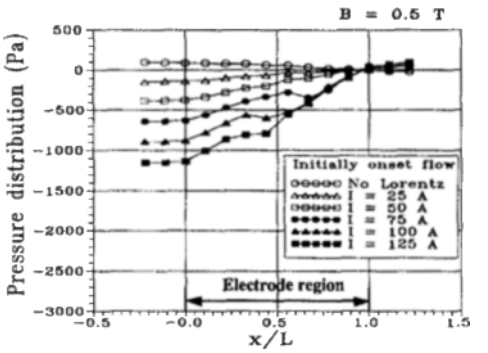


(a) B=0.5T

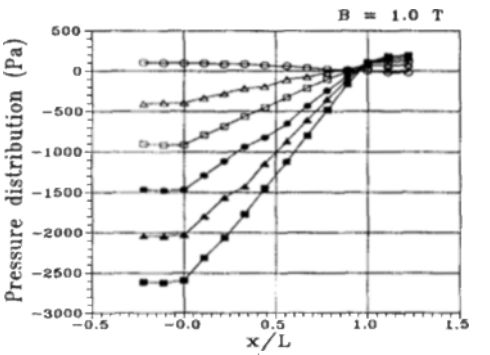


(b) B=1.0T

**Fig. 6** Pressure distribution in case of initially onset flow of the fan-shaped MHD thrust duct

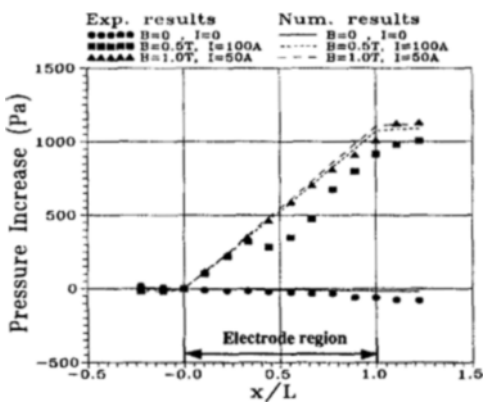


**Fig. 7** Experimental and numerical pressure distribution of the fan-shaped MHD thrust duct

an onset flow exists or not.

Figure 7 shows the comparisons of the pressures in the initially onset-flow case between the experimental and the numerical results. The measured pressure increase is less than that obtained from the numerical calculations. It is interesting to note that for the same Lorentz force the higher the magnetic flux density, the smaller the difference between the experimental and the numerical results. It can be conjectured that bubbles may cause these small differences in the pressure increase in the experiment, because the greater electricity generates more bubbles which cause a decrease in pressures.

Figure 8 shows the pressure difference between both ends of the duct with respect to the applied electric current for the rectangular and fan shaped, cross-sectional ducts. The experimental results for the rectangular duct was obtained previously (Kim, 1995). The solid symbols represent the fan-shaped, cross-section duct. The results show that the pressure of the fan-shaped cross-section duct is slightly smaller than the pressure increase of the rectangular cross-section

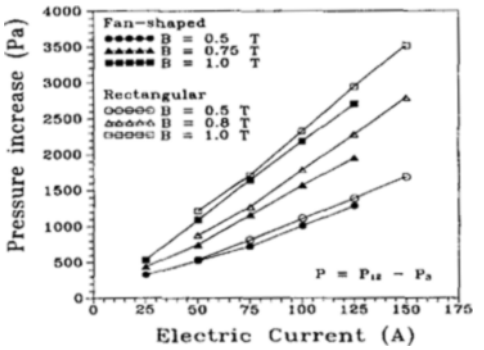


**Fig. 8** Pressure increases of the fan-shaped cross-section duct and of the rectangular cross-section duct due to the Lorentz force

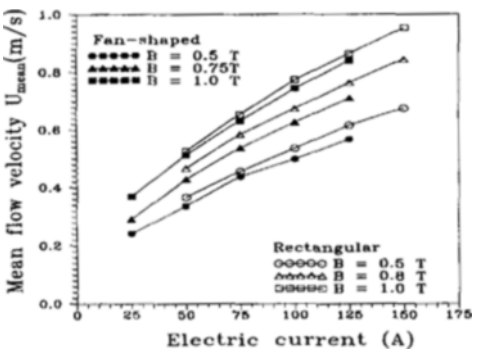


**Fig. 9** Mean velocity increases of the fan-shaped cross-section duct and of the rectangular cross-section duct due to the Lorentz force

duct. In the present experimental condition, the magnetic field is applied in vertical direction and the electric field is applied in circumferential direction. Therefore, the magnetic field and the electric field do not cross each other at right angles except for the center line of the duct. This non-orthogonal intersection of the electric field and the magnetic field produces lesser Lorentz force density and, hence, it may contribute to the differences of the pressure increase in the two cases.

As can be seen in Fig. 8, when the applied Lorentz force density is maintained constant, the pressure increase is larger in the stronger magnetic field than in the stronger electric field. Void fraction of the bubbles in the sea water could make the Lorentz force relatively small compared with the flow field without bubbles.

Figure 9 shows the mean velocity increase when the sea water in the duct is initially at rest. The mean velocity increase of the fan-shaped cross-section duct is found to be slightly less than that of the rectangular cross-section duct, similar to the pressure results. The relation between the velocity increase and the applied Lorentz force density is as follows:

$$\rho f_e \frac{U^2}{2} \frac{L_e}{D_e} = \Delta p = \sigma E_o B_o L \tag{7}$$

$$U^2 \propto \Delta p = \sigma E_o B_o L \tag{8}$$

where $f_e$ is the effective friction factor, $U$ the mean flow velocity, $L_e$ the effective length, $D_e$ the effective hydraulic diameter over the entire region of the propulsion duct and $\Delta p$ the pressure increase due to the applied Lorentz force.

### 6.2 Velocity distribution

Velocity measurement is carried out in the case of initially onset flow. In Fig. 10(a), (b) and (c), the velocity profiles of the experimental and numerical results for the fan-shaped and rectangular ducts at $B=0.5T$, $I=100A$ along the centerline ($z/W=0$) of the duct are presented. The solid line and solid symbol show the results of the fan-shaped duct while the dashed line and hollow symbol represent the results of the rectangular duct. The calculated Lorentz force density profile without showing the scales for the fan-shaped duct is also presented for comparison sake in Fig. 10(b) by the finely dashed line. Figure 11(a), (b) and (c) show the results at $B=1.0T$, $I=50A$.

As shown in the figure, the Lorentz force density decreases as it goes to the upper part of the fan-shaped, cross-section duct. The reason is that the distance of the electric current passage increases in the upper part due to the wider gap between the two electrodes, which results in lesser magnitude in $\boldsymbol{J}$ and, hence, lesser in the Lorentz force density. Such a trend is reflected in the velocity profiles of the fan-shaped duct.

The nose-shaped velocity profiles of the fan-shaped duct give a distinct contrast to those of the rectangular duct. The symmetry in cross-section

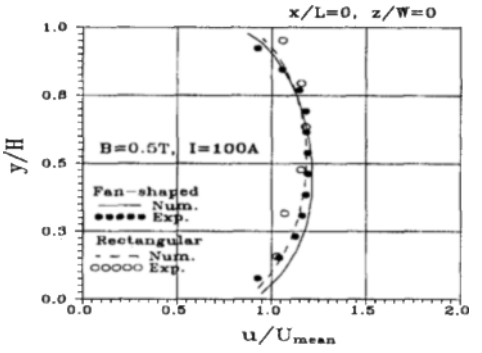


(a) $x/L=0$

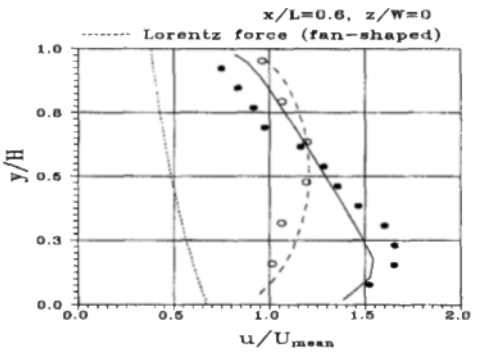


(b) $x/L=0.6$

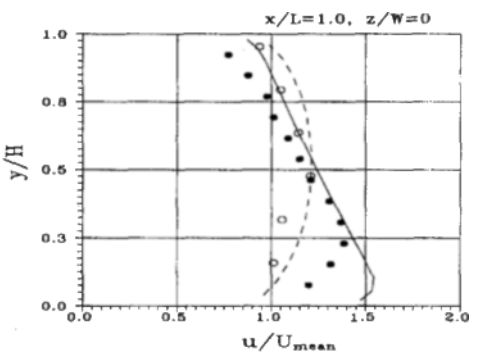


(c) $x/L=1.0$

**Fig. 10** Comparison of velocity distribution at B =0.5T, I=100A along the centerline of the duct, i. e. $z/W=0$ between the rectangular and fan-shaped ducts.

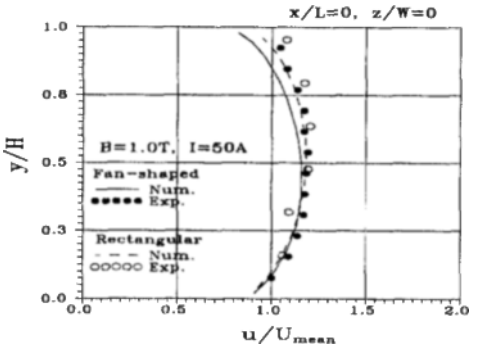


(a) $x/L=0$

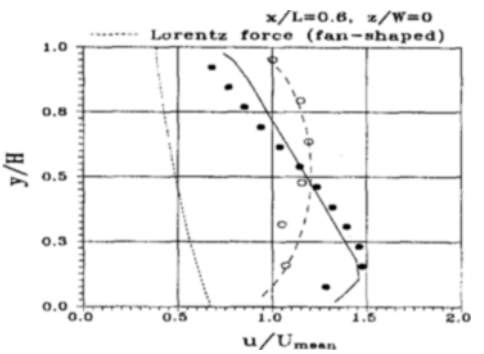


(b) $x/L=0.6$

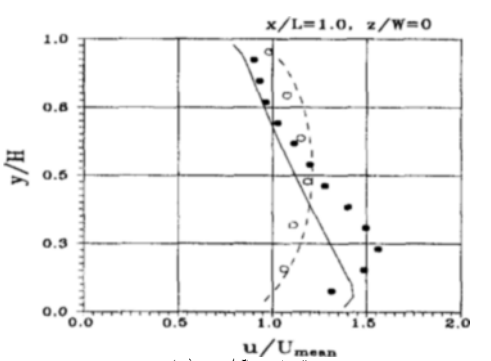


(c) $x/L=1.0$

**Fig. 11** Comparison of velocity distribution at B =1.0T, I=50A along the centerline of the duct, i. e. $z/W=0$ between the rectangular and fan-shaped ducts.

shape and in the Lorentz force density results in nearly symmetric velocity profiles of the rectangular duct, while such a symmetry is unrealized in the fan-shaped cross section except at the duct inlet. There, it appears that the Lorentz force has not developed to a full strength, and, thus, it fails to influence the velocity distinctively.

From Fig. 10, it is obvious the flow rate along

the longitudinal centerplane of the fan-shaped duct is greater than that of the rectangular duct. Since, the flow rates of the two ducts were kept constant, the flow velocities near the side walls of the fan-shaped duct should be smaller compared to those of the rectangular duct. This means that the stability of the flow in the fan-shaped duct could be worse compared to the rectangular duct.

One should note in Fig. 10 that the extent of the bulge in the velocity profile of the fan-shaped duct seems to decrease as the flow approaches the duct outlet. Such a trend seems to be reversed from $100A$ to $50A$ as shown in Fig. 11. The Lorentz force density was kept identical to obtain the results shown in Figs. 10 and 11. For the rectangular duct the variation of the velocity profiles at different locations and for different combinations of the magnitudes of $\boldsymbol{B}$ and $\boldsymbol{I}$ seems very small.

One can observe from Figs. 10 and 11 that the discrepancies between the experimental and computational results are larger for the fan-shaped duct and they are amplified as the flow goes downstream. Despite the fact that the present computational method does not account for the inhomogeneity of the fluid caused by the presence of bubbles, the agreement between the computational and experimental results are judged rather good. At this stage, one can only conclude that as more bubbles flow downstream the fluid in that region may become more bubbly for which the present computational method is incapable of yielding correct results.

The results obtained in the present investigation imply that the rectangular duct would be better suited for the purpose of MHD propulsion than the fan-shaped duct from the standpoint of flow stability and thrust efficiency.

## 7. Conclusion

From the comparison of the fan-shaped MHD propulsion duct with the rectangular cross-section duct, it can be inferred that the velocity profile is significantly influenced by the geometrical configuration due to the non-uniform Lorentz force density distribution, while the pressure field and the increase of the pressure along the flow direction of the duct are not so much affected as the velocity profile.

It can be inferred from the experiment that bubbles generated by electrolysis play an important role in influencing the flow characteristics in an MHD propulsion duct by changing the fluid density and the electric conductivity of the fluid.

## Acknowledgment

The authors acknowledge with gratitude the supports granted by Agency for Defense Development and Advanced Fluids Engineering Research Center of Pohang University of Science and Technology.

## References

Branover, H., 1978, *Magnetohydrodynamic Flow in Ducts*, Keter Publishing House, pp. 15~27.

Chen, Y. S., 1986, "A Computer Code for Three-Dimensional Incompressible Flows Using Non-Orthogonal Body-Fitted Coordinate Systems," *NASA* CR178818.

Doragh, R. A., 1963, "Magnetohydrodynamic Ship Propulsion Using Superconducting Magnets," *Transaction of SNAME*, Vol. 71.

Friauf, J. M., 1961, "Electromagnetic Ship Propulsion," *ASME J.*, pp. 139~142.

Hayt, W. H., Jr, 1989, *Engineering Electromagnetics,* McGraw-Hill, 5th edition, pp. 450~453.

Kim, C. T., 1995, "Investigation of Flow Characteristics of MHD Propulsion Ducts," *POSTECH M. S.* Thesis.

Launder, B. E. and Spalding, D. B., 1972, *Mathematical Models of Turbulence*, Academic Press, London.

Mine, S. and Ito, S., 1991, "Performance Test of Superconducting Magnet for YAMATO-1," *Proc. MHDS* 91, pp. 119~121.

Motora, S., et al., 1991, "An Outline of the R& D Project on Superconducting MHD Ship Propulsion in Japan," *Proc. MHDS 91*, pp. 53~68.

Phillips, O. M., 1962, "The Prospects for Magnetohydrodynamic Ship Propulsion," *Jour-*

*nal of Ship Research*, Vol. 43, pp. 43~51.

Rice, W. A., Aug. 22, 1961, U. S. Patent 2997013.

Saji, Y., Kitano, M. and Iwata, A., 1978, "Basic Study of Superconducting Electromagnetic Thrust Device for Propulsion in Sea Water," *Advances in Cryogenic Engineering*, K. D. Timmerhans, Ed., Vol. 23, pp. 159~169.

Swallom, D. W., et al., 1991, "Magnetohydrodynamic Submarine Propulsion Systems," *Naval Engineers Journal*, pp. 141~157.

Way, S., 1968, "Electromagnetic Propulsion for Cargo Submarines," *Journal of Hydronautics*, Vol. 2, pp. 49~57.

Weh, H., et al., 1991, "Ship Propulsion with Electromagnetic Direct Drives," *Proc. MHDS* 91, pp. 29~38.

Yang, O. C., 1994, "An Experimental Study on the Seawater Flow in the Rectangular Duct of MHD Thruster," *POSTECH M. S.* Thesis.